FRONTIER LETTER

Open Access

Rock-magnetic properties of single zircon crystals sampled from the Tanzawa tonalitic pluton, central Japan

Masahiko Sato[1,2*], Shinji Yamamoto[3], Yuhji Yamamoto[4], Yoshihiro Okada[5], Masao Ohno[2], Hideo Tsunakawa[5] and Shigenori Maruyama[6]

Abstract

This paper reports on the rock-magnetic properties of single zircon crystals, which are essential for future work establishing the reliable paleointensity method using single zircon crystals. Zircon crystals used in this study were sampled from the Nakagawa River, which crosses the Tanzawa tonalitic pluton in central Japan. Rock-magnetic measurements were conducted on 1037 grains of zircons, but many of these measurements are below the limits of the sensitivity of the magnetometers employed. Isothermal remanent magnetizations (IRMs) of 876 zircon crystal are below the practical resolution of this study; we infer that these crystals contain no or only minute quantities of ferromagnetic minerals. The other zircon crystals contain enough magnetic minerals to be measured in the DC SQUID magnetometer. For 81 zircon crystals, IRM intensities (M_{IRM}) are larger than 4×10^{-12} Am^2, while natural remanent magnetization (NRM) intensities (M_{NRM}) are below 4×10^{-12} Am^2, indicating that these crystals are inappropriate for the paleomagnetic study. For the samples that had values of $M_{NRM} \geq 4 \times 10^{-12}$ Am^2 and $M_{IRM} \geq 4 \times 10^{-12}$ Am^2 (80 zircons), combining the rock-magnetic parameter, we proposed the sample-selection criteria for future study of paleointensity experiments using single zircon crystals. In the case that the samples had high coercivity (B_c) values (>10 mT) or high M_{NRM}/M_{IRM} values (>~0.1), main remanence carriers are probably pyrrhotite and these samples are inappropriate for the paleointensity study. In the case that the samples had low B_c values (<10 mT) and low M_{NRM}/M_{IRM} values (<~0.1), main remanence carriers seem to be nearly pure magnetite with pseudo-single-domain grain sizes, and these samples are expected to appropriate for the paleointensity study. Total thermoremanent magnetization (TRM) acquisition experiments were also carried out for 12 samples satisfying the above criteria. The TRM intensity was comparable with that of NRM, and a rough estimation of the paleointensity using NRM/TRM ratios shows field intensities consistent with the average geomagnetic field intensity at the Tanzawa tonalitic pluton for last 5 Myr.

Keywords: Rock-magnetism; Paleointensity; Zircon; Tanzawa tonalitic pluton

Findings

Introduction

Geomagnetic field paleointensity data provide critical information about the thermal evolution of the Earth, and the state of the geomagnetic field has been proposed to be closely related to the surface environment (Tarduno et al. 2014). While it is pivotal to understand the variations in geomagnetic field intensity through the history of the Earth, data are still too scarce to a resolve billion-year-scale geomagnetic field variation. This is primarily due to the lack of well-preserved rocks for older eras, which often results in unsuccessful paleointensity experiments.

To overcome this problem, much research in recent years has focused on paleointensity experiments using single silicate crystals, which often accompany magnetic mineral inclusions, such as plagioclase (Tarduno et al. 2006 and references therein), quartz phenocryst (Tarduno et al. 2010), pyroxene (Muxworthy and Evans 2012), and olivine (Tarduno et al. 2012). Notably, the paleointensity method using single silicate crystals can be applied to the samples that failed paleointensity experiments using bulk

* Correspondence: m.satou@aist.go.jp
[1]Geological Survey of Japan, National Institute of Advanced Industrial Science and Technology, 1-1-1 Higashi, Tsukuba 305-8567, Japan
[2]Department of Environmental Changes, Faculty of Social and Cultural Studies, Kyushu University, 744 Motooka, Nishi-ku, Fukuoka 819-0395, Japan
Full list of author information is available at the end of the article

Sato *et al. Earth, Planets and Space* (2015) 67:150

Page 2 of 14

rock to obtain new, valuable information. However, some crystal types, such as plagioclase, pyroxene, and olivine, are easily influenced by alteration and metamorphism, and paleointensity experiments are still limited to the small number of samples.

This study focuses on zircon crystals. Zircon crystals play an important role in paleomagnetic studies because they have several mineralogical advantages: (1) they commonly occur in crustal rocks, (2) precise age determinations with U–Th–Pb and (U–Th)/He analyses are possible, and (3) they are highly resilient and may provide our only means to examine the oldest geomagnetic field (Tarduno et al., 2014, 2015). Recently Tarduno et al. (2015) demonstrated that paleointensity data of Archean to Hedean zircons bearing magnetic inclusions from the Jack Hills conglomerate could be used to reconstruct the early geodynamo. Although rock-magnetic properties of single zircon crystal are essential for future work establishing the reliable paleointensity method, systematic rock-magnetic studies have not been conducted for single zircon crystals, which is largely because of their small size and related weak magnetic moment.

This study conducts systematic rock-magnetic measurements using single zircon crystals that originated from the Tanzawa tonalite in central Japan. The materials in this region represent typical continental crust. Moreover, the crystals have young crystallization ages and a clear thermal history. We report the rock-magnetic properties of zircon crystals, and a preliminary result of thermoremanent magnetization (TRM) acquisition experiment for future study of paleointensity experiments using single zircon crystals.

Geology and sampling

Zircon crystals used in this study were sampled from fluvial sands of the Nakagawa River, which crosses the Tanzawa tonalitic plutons in central Japan (35° 26′ 05′′ N, 139° 02′ 44′′ E). A geological map around the Tanzawa block and Nakawaga River is shown in Fig. 1a. The Tanzawa block is situated in the Izu Collision Zone, where the Izu–Bonin–Mariana (IBM) arc has collided with the Honshu arc (Matsuda 1978; Niitsuma et al. 2003; Yamamoto et al. 2009). The IBM arc is believed to be the major site of continental crust formation. The seismic profiling of the IBM arc crust demonstrated the presence of a middle crust with the P wave velocity (V_p) of 6 km/s (Suyehiro et al. 1996; Takahashi et al. 2007). The V_p value corresponded to intermediate-to-felsic tonalitic composition, which is average chemical composition of the continental crust (e.g., Rudnick et al., 1995). The Tanzawa block is divided into three main geological units: (1) the Tanzawa Group (basaltic volcanoclastics), (2) the Tanzawa gabbro suite, and (3) the Tanzawa tonalitic plutons. According to previous studies, the Tanzawa tonalities can be regarded as the exposed middle crust of the former IBM arc (Suyehiro et al. 1996; Kawate and Arima 1998), and thus, the Tanzawa tonalitic pluton is generally considered to be a typical continental crust. The Tanzawa tonalities have very low K_2O, low K_2O/Na_2O ratios (Ishihara et al. 1976), and low initial $^{87}Sr/^{86}Sr$ ratios near mantle values (Kawate and Fujimaki 1996; Tamura et al. 2010); they are also enriched in magnetite with high magnetic susceptibility (Ishihara et al. 1976; Ishihara and Matsuhisa 1999).
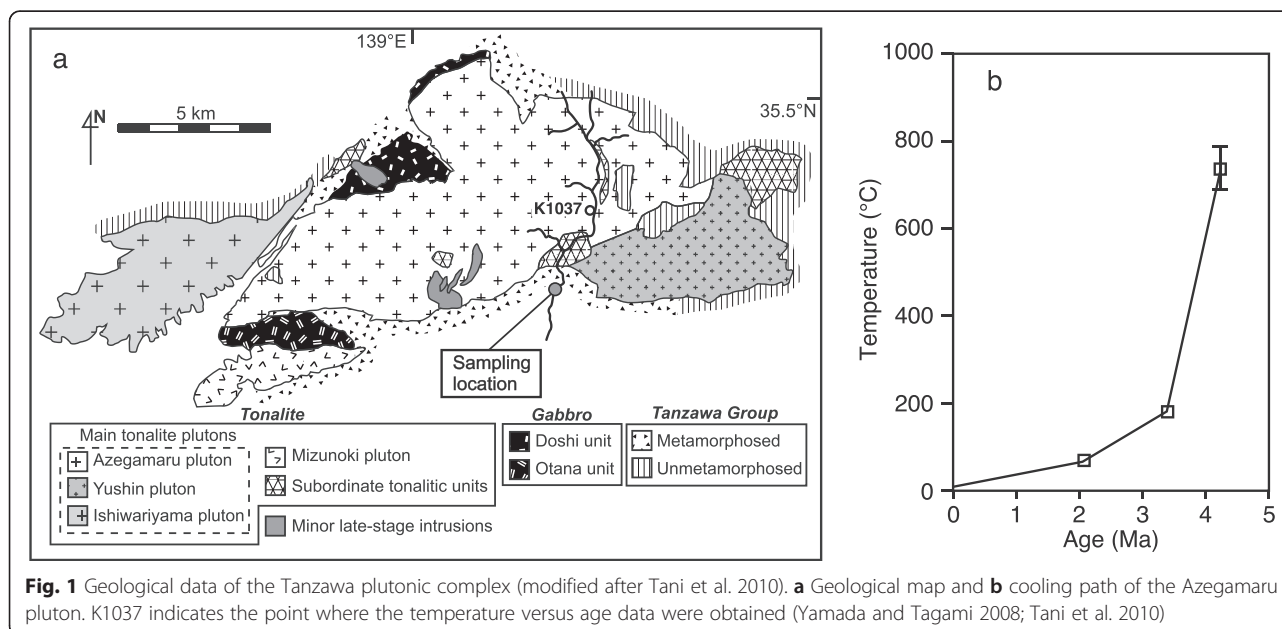
Fig. 1 Geological data of the Tanzawa plutonic complex (modified after Tani et al. 2010). **a** Geological map and **b** cooling path of the Azegamaru pluton. K1037 indicates the point where the temperature versus age data were obtained (Yamada and Tagami 2008; Tani et al. 2010)

Sato *et al. Earth, Planets and Space* (2015) 67:150

Page 3 of 14

The Nakagawa River flows along bodies of the Tanzawa plutonic complex. Since the fluvial sands were collected just downstream of the Azegamaru pluton (Fig. 1a), we can collect large amounts of coarse-grained zircon crystals that had originated from the Azegamaru pluton. Note that the zircon crystal collected at the point may contain a certain amount of zircon crystals that had originated from the subordinate tonalitic unit (Otakisawa unit). The Otakisawa unit formed between the Gabbroic unit and the Azegamaru pluton (Takita 1974). The zircon U–Pb ages in the Gabbroic unit were determined as ca. 5 Ma (Tani et al. 2010). The typical grain size of the Tanzawa zircon ranges from 50 to 200 μm (Suzuki et al. 2014), and we selectively collected coarse zircon crystals larger than 150 μm in size.

The zircon U–Pb ages in the Azegamaru pluton were determined as ca. 4–5 Ma using a sensitive high resolution ion micro probe and laser ablation-inductively coupled plasma mass spectrometry (Tani et al. 2010; Suzuki et al. 2014). Yamada and Tagami (2008) also reported (U–Th)/He zircon and apatite ages. On the basis of these results, post emplacement thermal history of the Azegamaru pluton can be estimated. The cooling rate of the Azegamaru pluton was calculated to be ~658 °C/Myr during the time span of 3–4 Ma (Fig. 1b), and Tani et al. (2010) pointed out that the Tanzawa plutonic complex is one of the most rapidly cooled granitic plutons on the Earth. It is worth noting that the Azegamaru pluton did not experience severe heating after the rapid cooling (Fig. 1b). The young crystallization ages and the clear thermal history make the Azegamaru pluton suitable for testing the feasibility of conducting a paleointensity experiment using single zircon crystals.

Methods

Zircon preparations

Heavy mineral fractions including zircon grains were concentrated from fluvial sands of the Nakagawa River using a panning method without magnetic-separation and heavy-liquid techniques to avoid any adverse effects on magnetic measurements. Later, the heavy fractions were sieved and arranged so that the samples were larger than 150 μm in size. Finally, zircon grains were hand-picked at random under a stereoscopic microscope for further analyses.

We collected 56 grains of zircon crystals to conduct a hydrochloric acid (HCl) leaching experiment. First, the 56 grains were placed together using a Scotch Magic Transparent Tape (3 M) and isothermal remanent magnetization (IRM) was imparted with a field of 140 mT. The IRM intensity (M_{IRM}) of the 56 crystals was then measured using a 2G 3-component DC SQUID magnetometer (model 755) at Kyushu University.

Subsequently, the zircon crystals were removed from the tape and soaked in HCl for 4 to 8 d (HCl leaching), and then, the crystals were washed with water. The 56 grains were placed together using the tape. The IRM was again imparted for the 56 crystals, and M_{IRM} was measured.

For the main series of magnetic measurements, 1037 grains of zircon crystals were collected and used after HCl leaching for 10 d. To characterize the zircon, X-ray fluorescence (XRF) measurements were conducted on the 1037 grains with X-ray spot sizes of 100 μm using an XGT-7000 X-ray Analytical Microscope (HORIBA Scientific) at Kyoto University. Note that XRF observations were conducted after natural remanent magnetization (NRM) measurements.

Remanence measurement using SQUID magnetometer

Remanence measurements were carried out using a 2G 3-component DC SQUID magnetometer (model 755–4.2 cm discrete sample system) at the Center for Advanced Marine Core Research (CMCR), Kochi University. We used a sample holder specially designed for zircon measurements. The holder was made of acrylonitrile butadiene styrene (ABS) and cylindrical form of 7 mm in diameter and 6 cm in length (Additional file 1: Figure S1). The sample holder was fixed in a stainless rod and inserted into a sensing region of the magnetometer. The zircon crystal was sandwiched between the two Scotch Magic Transparent Tapes of 5 × 5 mm (sandwiched sample) and set at an edge of the holder using the Scotch Double Sided Tape (3 M). To keep a sample orientation, we fixed the zircon crystal sandwiched between the Transparent Tapes from NRM measurement to end of demagnetization/remanence measurement processes. In a sequence of remanence measurements, the sample holder was fixed in the stainless rod, and we only changed the sandwiched sample at an edge of the holder.

The typical sample holder moment with the Double Sided Tape was ~3×10^{-11} Am^2, and specific axis of the magnetometer did not show larger noise. To calculate the sample moment, we subtracted the holder magnetization from each sample measurement. We carried out repeated measurements of the holder to estimate the detection limit of our method. The holder moment after subtracting the averaged holder moment showed variation of ~2×10^{-12} Am^2 (Additional file 1: Figure S2). Thus, the practical detection limit of sample moments in our method was estimated to be ~4×10^{-12} Am^2.

NRM and IRM measurements

For 1037 grains of zircon crystals, NRM intensity (M_{NRM}) was first measured. Then, IRM was imparted with a field of 1 T using pulse magnetizers (ASC Scientific IM-10-30 Impulse Magnetizer and Magnetic Measurements PPMP10), and the resultant IRM intensity

Sato *et al. Earth, Planets and Space* (2015) 67:150

Page 4 of 14

was measured. Note that the IRMs were imparted for ~70 samples at one time and were roughly imparted to the north direction. For 142 grains with M_{IRM} values larger than 5×10^{-12} Am^2, low-temperature demagnetization (LTD) treatment was further conducted, and the memory (IRM intensity after LTD treatment; $M_{IRM-LTD}$) was measured. In this treatment, the sandwiched sample was placed in a Dewar bottle filled with liquid nitrogen and equilibrated for 1 min. Then, the sample was kept at room temperature for 2 min.

Hysteresis loop measurements

Magnetic hysteresis loops were measured for 46 zircon crystals with $M_{IRM} \geq 1 \times 10^{-10}$ Am^2 and $M_{NRM} \geq 4 \times 10^{-12}$ Am^2 using a MicroMag 2900 Alternating Gradient Magnetometer (Princeton Measurements Corporation) at Kyushu University. We used a P2 AGM transducer probe with a silica sample stage (Princeton Measurements Corporation). A saturation magnetization (M_s) of the probe was typically ~100 pAm^2 (Additional file 1: Figure S3). Prior to the zircon sample measurements, a hysteresis loop of the probe was measured to obtain data for a probe correction. In the zircon measurements, the hysteresis loop of the probe was subtracted from the measured hysteresis loop (probe + zircon sample) to calculate the magnetization of the zircon sample. The maximum field in the hysteresis loop measurement was 500 mT. For characterizations of the hysteresis parameters, a diamagnetic/paramagnetic correction was performed by subtracting the average slopes at the applied field of $|B| > 300$ mT. Coercivity (B_c) was determined by a second-degree polynomial interpolation. M_s was the average of the magnetizations for $|B| > 300$ mT.

Stepwise alternating field demagnetization and low-temperature magnetometry

To further investigate the magnetic properties of the zircon crystals, stepwise alternating field demagnetization (AFD) experiment and low-temperature remanence measurements were carried out for 12 zircon crystals. We prepared four sets of samples, which had M_{NRM}/M_{IRM} values of ~0.01, ~0.05, ~0.1, and ~1. For the 12 zircon crystals, the stepwise AFD were carried out on 1 T-IRMs after the LTD treatment with steps at 2, 4, 6, 8, 10, 12, 14, 16, 18, 20, 22.5, 25, 27.5, 30, 35, 40, and 45 mT. The AFD was performed using a DEM-95C alternating field demagnetizer (Natsuhara-Giken) with the two-axis tumbling system. Subsequently, using an MPMS-XL5 Magnetic Property Measurement System (Quantum Design) at CMCR, Kochi University, low-temperature remanence measurements were conducted for the 12 grains. This involved (1) thermal demagnetization during zero-field warming (ZFW) for an IRM imparted with a field of 2.5 T at 10 K after zero-field cooling from 300 K (ZFC

remanence) and (2) thermal demagnetization during ZFW for a remanence given by field cooling from 300 to 10 K with a field of 2.5 T (FC remanence).

Results

Zircon preparation

Representative photo images of the zircon crystals are shown in Fig. 2. It can be seen that the crystals have stubby euhedral shapes with colorless or pale pink, which are common characteristics of Tanzawa tonalites (Tani et al. 2010; Suzuki et al. 2014). All the crystals used in the magnetic measurements also showed a clear peak for zirconium in the XRF measurements. It was concluded that the 1037 crystals can be classified as zircons based on the stereoscopic microscope and XRF observations.

The IRM intensity decreased during HCl leaching for 4 d and was nearly constant after 4 d (Additional file 1: Figure S4). It is thought that surficial contamination of magnetic minerals can be removed by HCl leaching for 4 d, as previously reported by Lewis and Senftle (1966). Our main series of experiments were conducted on 1037 grains of zircon crystals that were subjected to HCl leaching for 10 d, thus they were most likely not affected by any surficial contamination.

NRM, IRM measurements

Results of the NRM and IRM measurements are shown in Fig. 3. Although the NRM intensity of the single zircon crystals varied from 10^{-13} to 10^{-9} Am^2, the practical detection limit of sample moments was ~4×10^{-12} Am^2, and the cluster of points below the limit is an artifact of magnetometer resolution rather than any special characteristic of the zircons. For 85 crystals (8.2 %), NRM intensities were larger than 4×10^{-12} Am^2. The IRM intensities of the single zircon crystals also varied by four orders of magnitude, and 161 crystals (15.5 %) had IRM intensity larger than 4×10^{-12} Am^2.

The LTD memory of IRM ($100 \times M_{IRM-LTD}/M_{IRM}$) is plotted as a function of IRM intensity in Fig. 4a. A portion of the samples with M_{IRM} values less than 1×10^{-11} Am^2 showed a LTD memory of IRM that was larger than 100 %, which was due to measurement errors. For the samples with values of $M_{IRM} \geq 1 \times 10^{-11}$ Am^2, there was no clear correlation between the M_{IRM} and $100 \times M_{IRM-LTD}/M_{IRM}$ (correlation coefficient approximately -0.22). The LTD memories of IRM were mainly distributed in the range of 50–70 % (Fig. 4b). The decrease in the IRM intensity after LTD treatment suggests the existence of nearly pure magnetite (Heider et al. 1992).
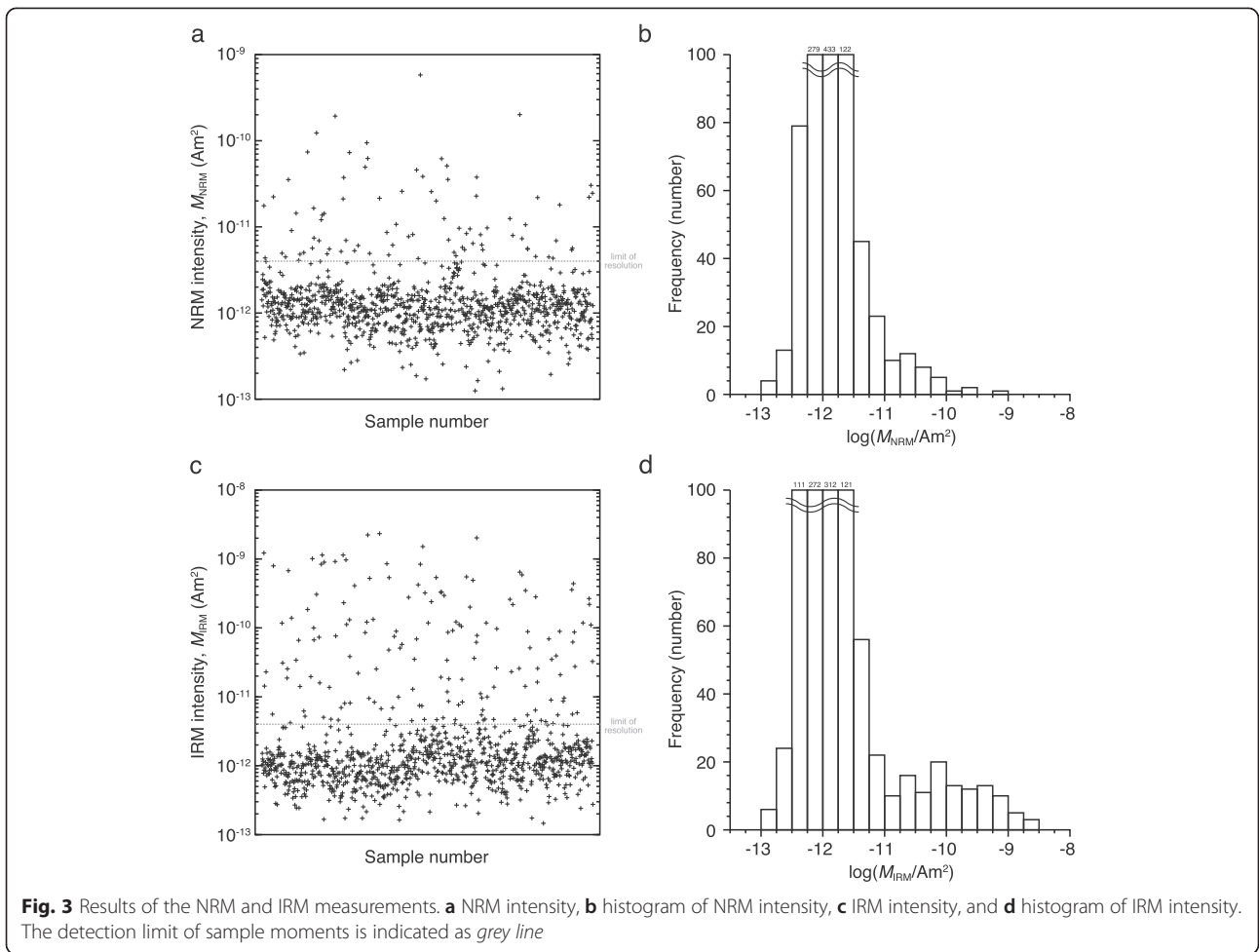
Hysteresis loop measurements

Typical examples of the magnetic hysteresis loops before and after slope correction are shown in Fig. 5a–d.

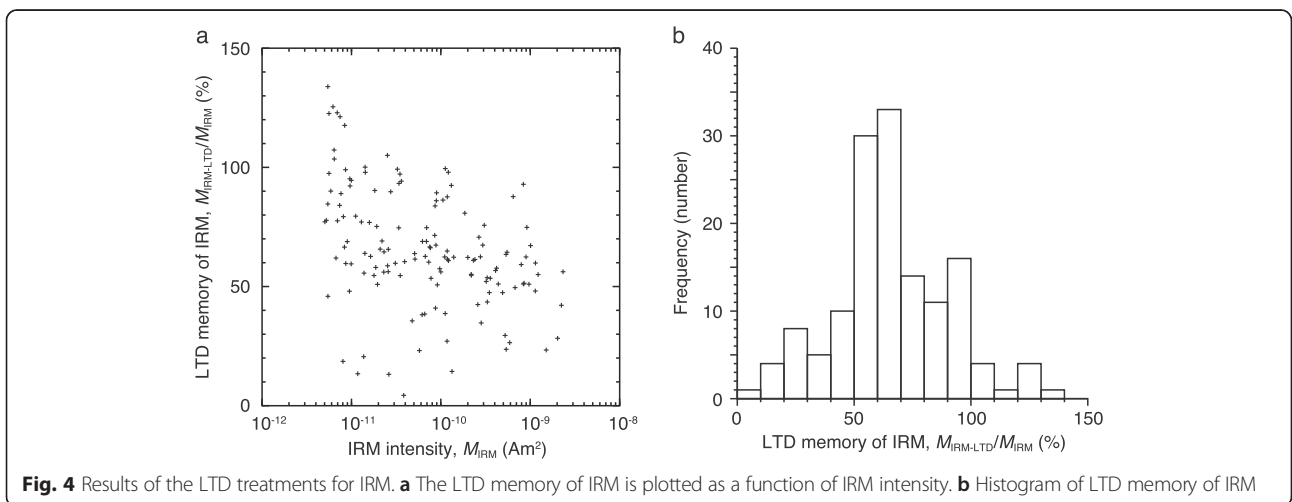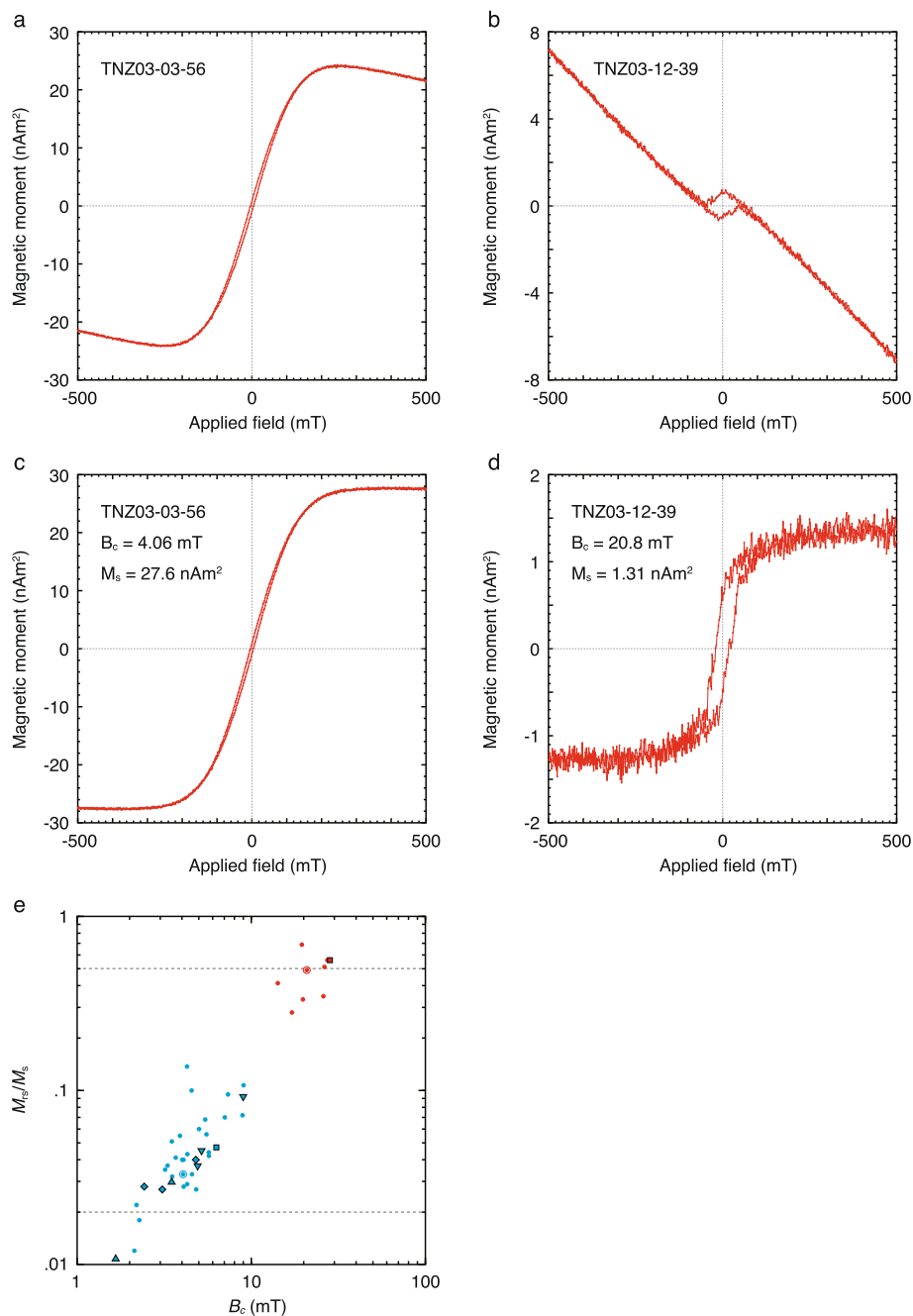Sato *et al. Earth, Planets and Space* (2015) 67:150

Page 5 of 14
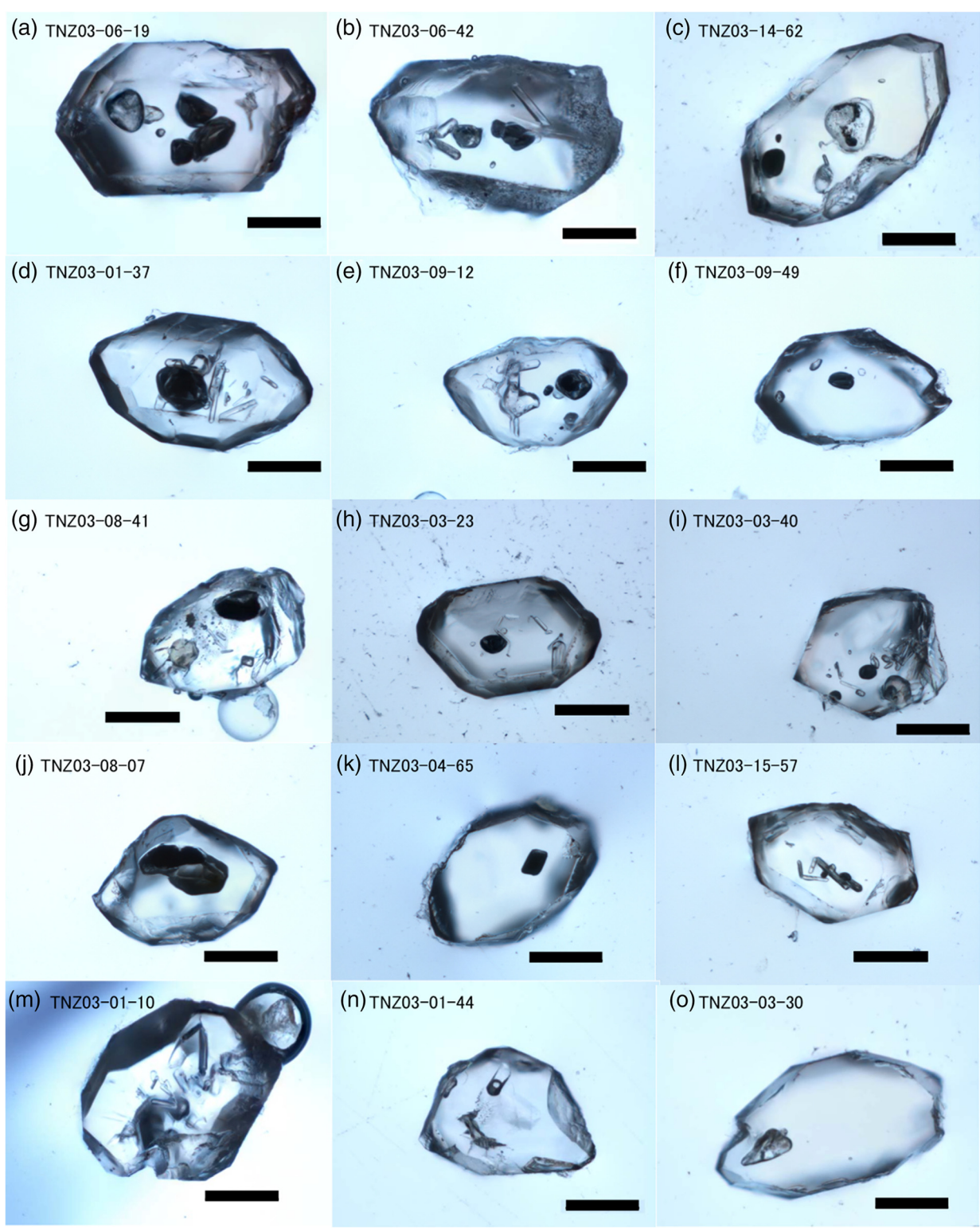
Fig. 2 Photo images of zircon crystals. The images are composite image of several photos which were taken at different depth of focus. *Scale bars* are 100 μm. The M_{NRM}/M_{IRM} values are **a–c** ~0.01, **d–f** ~0.05, **g–i** ~0.1, and **j–l** ~1. **m–o** The M_{IRM} values are lower than the detection limit (see text)

Sato *et al. Earth, Planets and Space* (2015) 67:150

Page 6 of 14

Fig. 3 Results of the NRM and IRM measurements. **a** NRM intensity, **b** histogram of NRM intensity, **c** IRM intensity, and **d** histogram of IRM intensity. The detection limit of sample moments is indicated as *grey line*

In order to evaluate the precision of the measurements, we calculated the standard deviation of M_s (σ_{Ms}) for $|B| > 300$ mT. The σ_{Ms} values were calculated to be ~100 pAm^2 for all samples. Because the M_s values should be constant in the hysteresis measurements, it is reasonable to consider that the induced magnetizations can be measured with ~100 pAm^2 precisions. The standard errors of M_s (δ_{Ms}) were calculated to be ~5 pAm^2 because of the stacking of ~400 points in M_s calculation. Thus, signal to noise ratios for M_s that

Fig. 4 Results of the LTD treatments for IRM. **a** The LTD memory of IRM is plotted as a function of IRM intensity. **b** Histogram of LTD memory of IRM

Sato *et al. Earth, Planets and Space* (2015) 67:150

Page 7 of 14

Fig. 5 Results of magnetic hysteresis measurements. **a–d** Examples of the hysteresis loops. The SD-like sample **a** before and **c** after the diamagnetic/paramagnetic correction. The PSD-like sample **b** before and **d** after the diamagnetic/paramagnetic correction. **e** The M_{rs}/M_s is plotted as a function of B_c. *Grey lines* indicate M_{rs}/M_s values of 0.5 and 0.02, which are representative values for SD/PSD and PSD/MD boundaries (Dunlop 2002). Data from the hysteresis loops in **c** and **d** are shown as *double circles*. The selected samples are shown as *inverted triangle, diamond, triangle,* and *square symbols* (see Fig. 6)

based on the δ_{Ms} values relative to the sample M_s ranged from 46 to 12,000. The B_c values varied from 1 to 30 mT, and the standard errors for B_c calculated from the second-degree polynomial fitting were typically ~10 % (Additional file 1: Tables S1 and S2). Since the B_c values for all samples were lower than 30 mT, it is reasonable to consider that the IRM imparted with a field of 1 T is close

to the saturation IRM (SIRM). For most of the samples, the noise of ~100 pAm^2 was too large to estimate a saturation remanent magnetization (M_{rs}). To precisely calculate the M_{rs}/M_s ratio, the M_{IRM} obtained from the IRM measurements was used as the M_{rs} value.

The magnetic hysteresis parameters of the single zircon crystals are plotted over the M_{rs}/M_s versus B_c plots (Tauxe

Sato *et al. Earth, Planets and Space* (2015) 67:150

Page 8 of 14

et al. 2002) in Fig. 5e. Representative M_{rs}/M_s values for single-domain (SD)/pseudo-single-domain (PSD) and PSD/ multidomain (MD) boundaries in the plots by Day et al. (1977) are also shown in Fig. 5e (Dunlop 2002). The SD- and PSD-like groups can be seen in this plot. Although the SD-like samples had low M_s values and the signal to noise ratios of the SD-like samples were lower than those of the PSD-like samples, the signal to noise ratios (>46) were large enough to distinguish these two groups.

Stepwise AFD

The stepwise AFD results are summarized in Fig. 6 and Additional file 1: Table S1. Magnetization of the samples with M_{NRM}/M_{IRM} values of ~0.01, ~0.05, and ~0.1 systematically decreased to the origin, as can be clearly seen in the orthogonal vector plots (Fig. 6a–c). On the other hand, the zircon crystals with M_{NRM}/M_{IRM} values of ~1 did not trend to the origin and showed unstable behavior during the AFD treatment (Fig. 6d). The normalized AFD curves are summarized in Fig. 7. The AFD curves are similar in shape for the samples with M_{NRM}/M_{IRM} values of ~0.01, ~0.05, and ~0.1, whereas dissimilar shapes were observed among the samples with M_{NRM}/M_{IRM} values of ~1. These results suggest that the main IRM carriers of the samples with M_{NRM}/M_{IRM} values of ~0.01, ~0.05, and ~0.1 and with M_{NRM}/M_{IRM} values of ~1 have different characteristics.

Low-temperature magnetometry

Results of the low-temperature remanence measurements are summarized in Fig. 8 and Additional file 1: Table S1. Most of the samples, except the two samples with M_{NRM}/M_{IRM} values of ~1 (TNZ03-04-65 and TNZ03-15-57), showed pronounced remanence reductions at around 100–150 K, which is suggestive of the Verwey transition for low-Ti titanomagnetite (Özdemir et al. 1993; Moskowitz et al. 1998). The smooth variation of remanences near 100–150 K indicated some impurities in magnetite grains. The curves also showed remanence reductions at ~35 and ~50 K, which may indicate the existence of magnetic minerals other than magnetite, such as pyrrhotite (Dekkers et al. 1989) and the rhombohedral phase of Fe–Ti oxide (Ishikawa et al. 1985). The apparent transitions of ~50 K were seen in most of the samples. If this transition indicates the rhombohedral phase of Fe–Ti oxide, it does not have remanent magnetization at room temperature. One sample (TNZ03-08-41) showed clear transition temperature ~35 K. If this transition indicates the pyrrhotite, it has remanent magnetization at room temperature and may affect paleointensity experiment. The intensity of FC remanence was larger than that of ZFC remanence, which is a characteristic behavior of SD and fine-grained PSD magnetite (Moscowitz et al. 1993; Kosterov 2003; Carter-Stiglitz et al. 2006), although the zircon crystals may contain magnetic minerals other than pure magnetite.

Sample-selection criteria for future study of paleointensity experiments

In this study, we carried out the systematic rock-magnetic measurements for the 1037 single zircon crystals using the standard magnetometers such as SQUID magnetometer, MPMS, and AGM. Combining the observed rock-magnetic parameters, we discuss sample-selection criteria for future study of paleointensity experiments using single zircon crystals.

The relationship between the M_{NRM} and M_{IRM} is shown in Fig. 9a. The samples that had M_{IRM} smaller than the practical detection limit of the instrument used in this study (876 zircons) are considered to contain little or no magnetic minerals. The other zircon crystals contain enough magnetic minerals to be measured in the DC SQUID magnetometer. The zircon crystals that had $M_{IRM} \geq 4 \times 10^{-12}$ Am^2 while M_{NRM} smaller than the detection limit (81 grains) are inappropriate for the paleomagnetic study. For the samples that had values of $M_{NRM} \geq 4 \times 10^{-12}$ Am^2 and $M_{IRM} \geq 4 \times 10^{-12}$ Am^2 (80 grains), the M_{NRM}/M_{IRM} ratios were distributed in the range of 0.004–0.8, excepting one anomalous sample with M_{NRM}/M_{IRM} value of ~1.5. This anomalously high M_{NRM}/M_{IRM} value is considered to arise from strong anisotropy of the crystal. In the stepwise AFD curves of the IRM after LTD treatment, the samples with low M_{NRM}/M_{IRM} value (~0.01, ~0.05, and ~0.1) show the stable remanent magnetizations, while the samples with high M_{NRM}/M_{IRM} value (~1) show unstable behaviors. Thus, in terms of room temperature IRM properties, the samples with low M_{NRM}/M_{IRM} value are desirable for paleointensity experiment.

Some large inclusions in the zircon crystals can be recognized from stereoscopic microscope observations (Fig. 2). The samples that had measureable IRM and NRM intensities tended to contain colored mineral inclusions (Fig. 2a–l and Additional file 1: Table S1), while the samples that had both IRM and NRM intensities smaller than the detection limit rarely contain colored minerals (Fig. 2m–o). Tanzawa tonalites mainly consist of plagioclase, hornblende, quartz, and biotite with minor amounts of K-feldspar, chlorite, magnetite, ilmenite, ± actinolite, ± muscovite, ± cummingtonite, and ± tremolite (Suzuki et al. 2014). Note that the "±" denotes the way of description for minor minerals in the thin-section. In the petrology, the rock-forming minerals are described in descending order, and one thin-section sometimes contain the minor minerals but other times lack them even in the same rock sample. In such cases, the minor minerals would be represented as "±". Assuming that inclusions are the same as the tonalite, the probable candidates of the colored minerals are biotite, magnetite, ilmenite, and amphiboles, and those of the transparent minerals are plagioclase and quartz. Moreover, from preliminary electron microscope observations, we
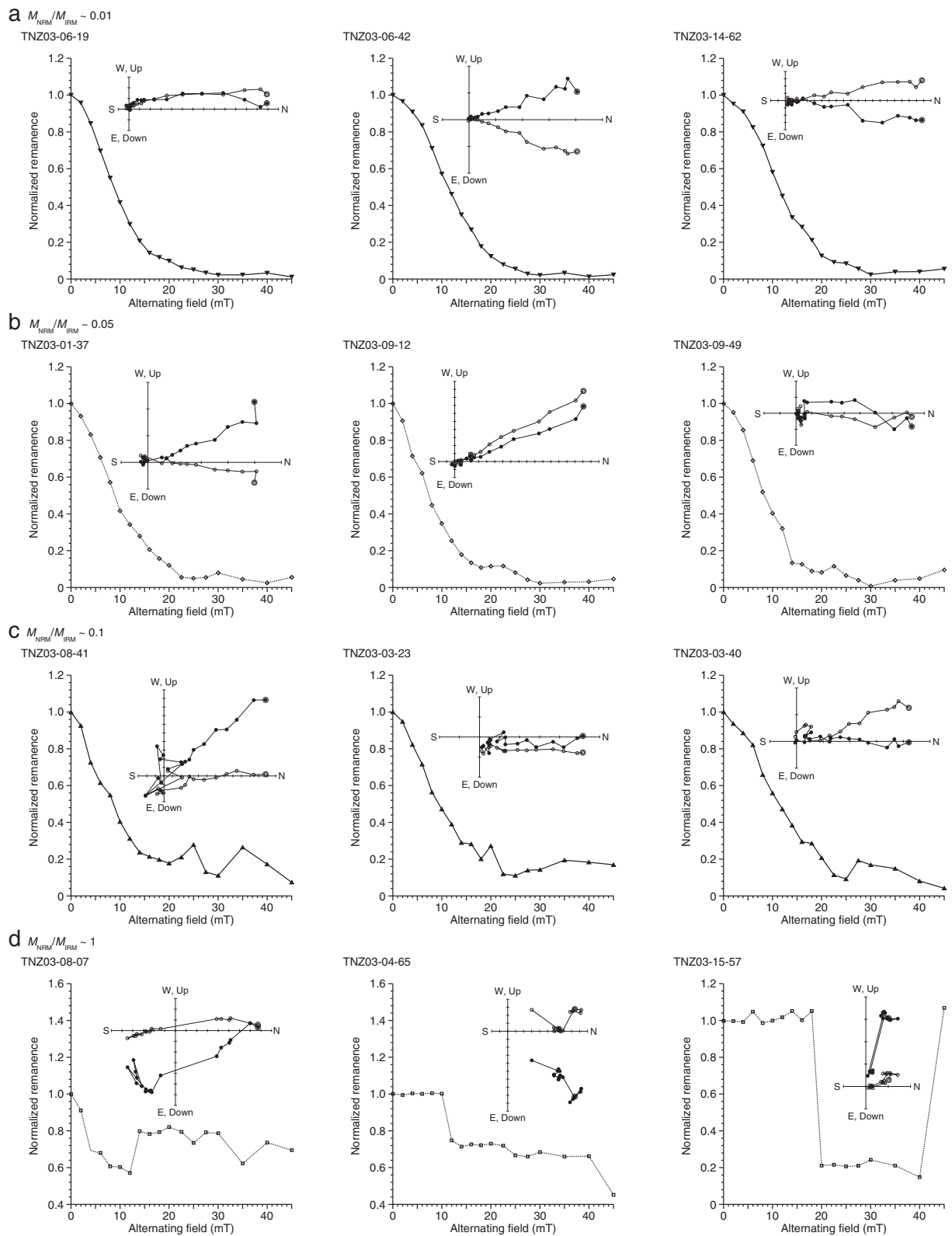
Sato *et al. Earth, Planets and Space* (2015) 67:150

Page 9 of 14

Fig. 6 (See legend on next page.)

Sato *et al. Earth, Planets and Space* (2015) 67:150

Page 10 of 14

found that the samples with M_{NRM}/M_{IRM} values of ~1 contain pyrrhotite crystals (TNZ03-04-65 and TNZ03-15-57) and the TNZ03-08-07 sample contains both magnetite and pyrrhotite crystals. Relationships between the types of magnetic properties and mineral inclusions should be investigated by a future study of detailed microscopic observations.

The M_{NRM}/M_{IRM} ratios are plotted as a function of B_c in Fig. 9b. In this plot, the values M_{NRM}/M_{IRM} and B_c tend to indicate magnetic properties of main carrier for remanent magnetization and induced magnetization, respectively. Taking into account the result of microscope observations and low-temperature magnetometry, magnetic minerals contained in the samples with high B_c values (>10 mT) are likely small numbers of pyrrhotite. If this is the case, main carriers for both remanent and induced magnetization were the small numbers of pyrrhotite, which is consistent with the stepwise change in remanence during AFD treatment and the high B_c values.

From the electron microscope observation and low-temperature measurement, we found that TNZ03-08-41 ($B_c = 1.7$ mT, $M_{NRM}/M_{IRM} = 0.1$) and TNZ03-08-07 ($B_c = 6.3$ mT, $M_{NRM}/M_{IRM} = 0.7$) contained both magnetite and pyrrhotite. The samples with low B_c values (<10 mT) and high M_{NRM}/M_{IRM} values (>~0.1) may

Fig. 7 Summary of the stepwise AFD curves for the selected zircon samples

contain nearly pure magnetite and small numbers of pyrrhotite. The large induced magnetization of the magnetite over the small numbers of pyrrhotite dominates hysteresis properties, while the small numbers of pyrrhotite efficiently carry the remanent magnetization and dominates remanence properties.

The samples with low B_c values (<10 mT) and low M_{NRM}/M_{IRM} values (<~0.1) showed (1) decrease in the IRM intensity after LTD treatment (Fig. 9c), (2) pronounced low-temperature remanence reduction at around 100–150 K (Fig. 8), (3) PSD-like M_{rs}/M_s values, and (4) relatively stable behavior during stepwise AFD treatment (Fig. 6). The features (1) and (2) suggest the existence of titanomagnetite. Considering the slow cooling rate of the Azegamaru pluton (Fig. 1b), it is unlikely that Ti-rich titanomagnetite existing in zircon crystals, and thus, the main magnetic mineral of these samples is nearly pure magnetite with PSD grain sizes.

In the present study, we did not measure the magnetic anisotropy. Unlike feldspars or pyroxenes, there is no apparent reason to believe that exsolution should be a common process in zircon. Therefore, anisotropy is not expected, but it could be present if the magnetization is dominated by small numbers of inclusions such as the pyrrhotite-bearing samples (high B_c values of >10 mT or high M_{NRM}/M_{IRM} values of >~0.1).

In the case that the samples had high B_c values (>10 mT) or high M_{NRM}/M_{IRM} values (>~0.1), main remanence carriers are probably pyrrhotite, and these samples are inappropriate for the paleointensity study. In the case that the samples had low B_c values (<10 mT) and low M_{NRM}/M_{IRM} values (<~0.1), the main remanence carrier seems to be nearly pure magnetite with PSD grain sizes. These samples showed the moderate LTD memories of IRM (50–70 %, Fig. 9c) and relatively stable behavior during stepwise AFD treatment (Fig. 6). The 50 µT-TRM/SIRM ratios for pure PSD magnetite ranged from 0.006 to 0.1 (Figure 1b in Yu 2010); the NRMs of the sample with M_{NRM}/M_{IRM} values of <~0.1 may have a TRM origin. Thus, the samples had low B_c values (<10 mT) and low M_{NRM}/M_{IRM} values (<~0.1) are expected to be appropriate for the paleointensity study. The threshold value of M_{NRM}/M_{IRM} ~0.1 is tentative, and it would be better to select the sample with sufficiently small M_{NRM}/M_{IRM} values such as <~0.05. In addition, it is worth noting that the data shown here are much more complicated than other single silicate results

Sato *et al. Earth, Planets and Space* (2015) 67:150

Page 11 of 14
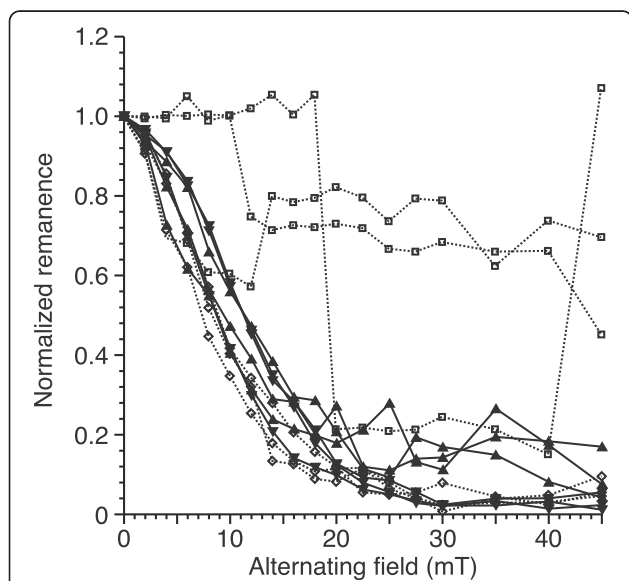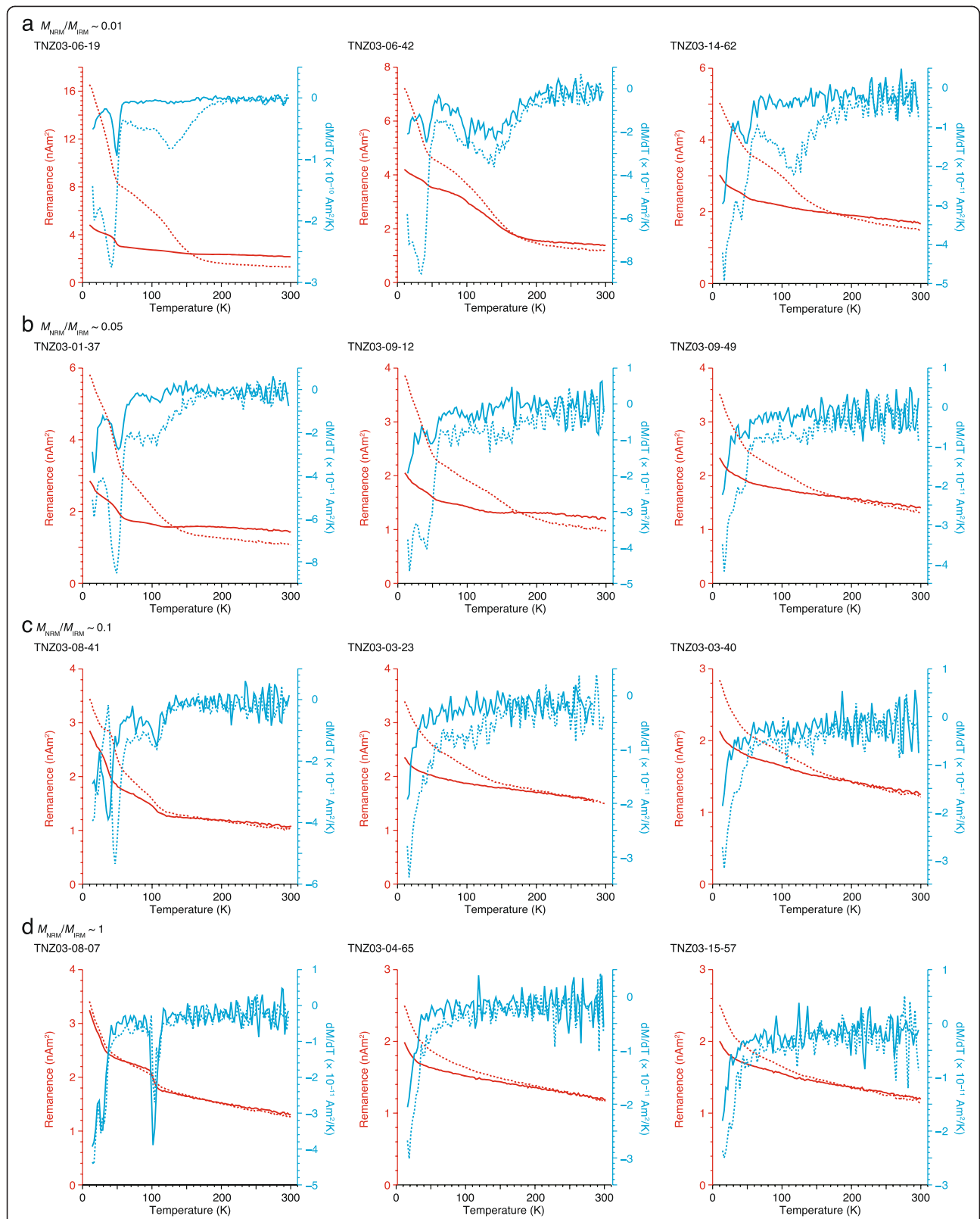
Fig. 8 Results of low-temperature remanence measurements for the selected zircon samples. The ZFC remanence and FC remanence curves are shown with *red color* as *bold* and *dot lines*, respectively. Temperature derivatives of the ZFC remanence and FC remanence curves are shown with *blue color* as *bold* and *dotted lines*, respectively

Sato *et al. Earth, Planets and Space* (2015) 67:150

Page 12 of 14
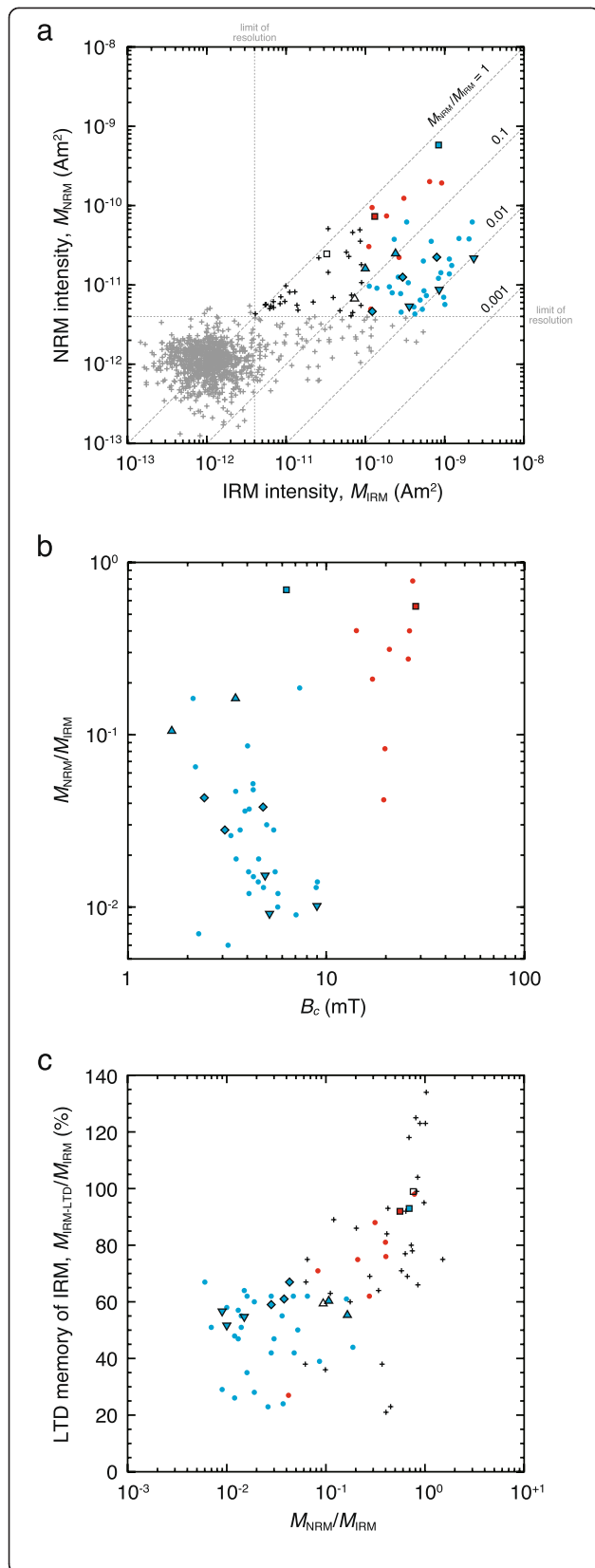
Fig. 9 a The NRM intensity is plotted as a function of the IRM intensity. *Diagonal lines* indicate IRM/NRM ratios of 1, 0.1, 0.01, and 0.001, respectively. Vertical and horizontal *grey lines* indicate 4×10^{-12} Am^2 intensity lines (detection limit). The sample with $M_{IRM} < 4 \times 10^{-10}$ Am^2 or $M_{NRM} < 4 \times 10^{-12}$ Am^2 are shown as *grey symbols*. **b** The NRM/IRM ratio is plotted as a function of B_c. **c** The LTD memory of IRM is plotted as a function of the NRM/IRM ratio. The SD- and PSD-like samples are plotted as *red* and *blue symbols*, respectively (see Fig. 5). The selected samples are shown as *inverted triangle, diamond, triangle*, and *square symbols* (see Fig. 6)

so far reported, and thus, rock-magnetic investigations with large number of crystals similar to this study would be necessary to provide solid ground for single silicate crystal paleomagnetism, including feldspar or quartz.
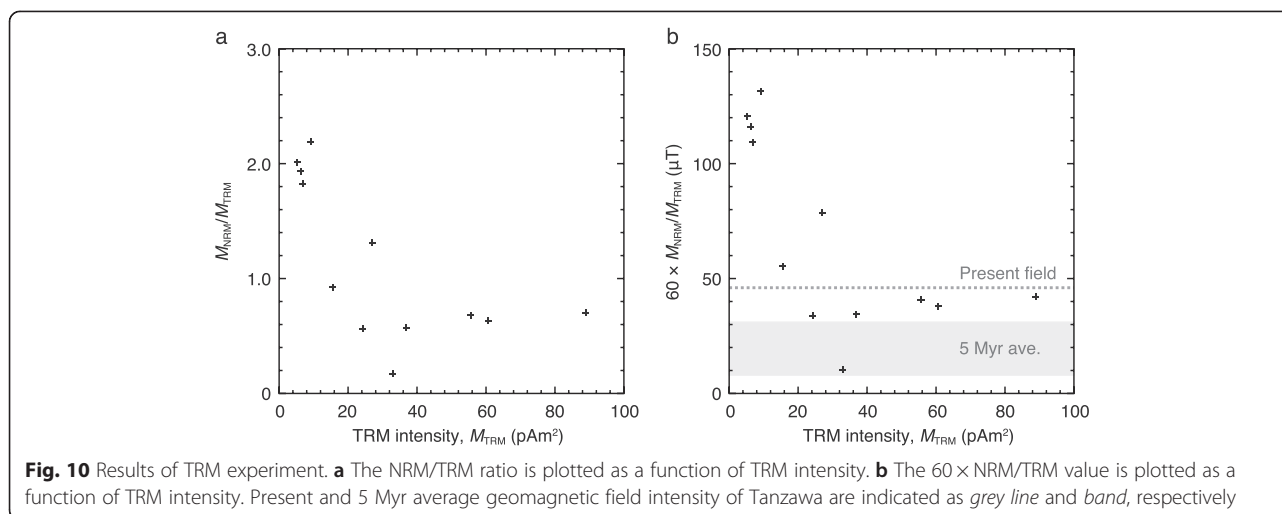
TRM experiments—implication for paleointensity experiment

Toward the establishment of a reliable paleointensity method using single zircon crystal, we selected 13 zircon crystals with M_{NRM}/M_{IRM} values of 0.01–0.05 and low B_c values of <10 mT and used these in a TRM acquisition experiment. The TRM was imparted by heating crystals to 610 °C for 15 min and cooling them back to room temperature with a 60-μT DC field. The heating procedures were conducted in a vacuum (<10 Pa) with a TDS-1 thermal demagnetizer (Natsuhara-Giken). One of the 13 crystals broke during the heating procedure. The TRM intensities (M_{TRM}) of the remaining 12 crystals were measured using the model 755 cryogenic magnetometer at CMCR, Kochi University.

Results of the TRM experiment are summarized in Fig. 10 and Additional file 1: Table S2. The NRM/TRM ratios varied from 0.2 to 2.2 (Fig. 10a), indicating that the NRM intensity is comparable to the TRM intensity. For the crystals with $M_{TRM} \geq 10$ pAm^2, an average of M_{NRM}/M_{TRM} values was 0.69. This corresponds to 41 μT if we roughly estimate possible paleointensity because we imparted TRM with a 60-μT DC field (Fig. 10b).

Considering an average virtual axial dipole moment of $3.64 \pm 2.10 \times 10^{22}$ Am^2 for the last 5 Myr concluded by Yamamoto and Tsunakawa (2005), the geomagnetic field intensity at the Tanzawa tonalitic pluton (35° 26′ N) has been estimated to be 8–31 μT for that period. This is comparable to the rough estimate of 41 μT in the present study, which suggests that the selected zircon crystals hold NRMs with a TRM origin, while (thermo) chemical remanent magnetization or (thermo) viscous remanent magnetization may well be plausible origins of NRM in the zircon crystals. Moreover, the slow cooling rate of the Azegamaru pluton (~658 °C/Myr) may affect the paleointensity estimate. The effect of cooling rate on TRM intensity is dependent on the grain size of magnetite. Yu (2011) tested the practical effect of cooling rate on the magnitude of TRM using natural and synthetic magnetite.

Sato *et al. Earth, Planets and Space* (2015) 67:150

Page 13 of 14

Fig. 10 Results of TRM experiment. **a** The NRM/TRM ratio is plotted as a function of TRM intensity. **b** The 60 × NRM/TRM value is plotted as a function of TRM intensity. Present and 5 Myr average geomagnetic field intensity of Tanzawa are indicated as *grey line* and *band*, respectively

As the results, TRM intensity of SD samples decrease as the cooling rate increases, while MD samples showed an opposite trend. TRM intensity of PSD samples remain almost unchanged as the cooling rate decreases. As the zircon crystals used in the TRM experiment showed the PSD-like hysteresis parameters which were close to the PSD/MD boundary (Fig. 5e and Additional file 1: Table S2), the roughly estimated paleointensity value of 41 μT was considered to be lower bound.

Considering the thermal history of the Azegamaru pluton (Fig. 1b), it is expected that a future study using the zircon crystals with low B_c values (<10 mT) and low M_{NRM}/M_{IRM} values (<~0.1) could provide reliable paleointensity data of the Tanzawa at ~3–4 Ma. Note that, for the future paleointensity experiment using single zircon crystal, it would be necessary to conduct more detailed analyses of zircon crystals such as (a) thermomagnetic analysis, (b) checking stability against heating, (c) direct observation of inclusions, and (d) NRM directional consistency tests using in-situ zircons in the tonalite.

Conclusions

In this study, we conducted a suite of rock-magnetic experiments for 1037 single zircon crystals sampled from the Nakagawa River, which crosses the Tanzawa tonalitic pluton in central Japan. The zircon crystals originated from the Azegamaru pluton, where the thermal history is clearly known. The IRM intensities for 876 zircon crystals were smaller than the practical detection limit of the instrument used in this study (~4 × 10^{-12} Am^2); these crystals contain no or only minute quantities of ferromagnetic minerals. The other zircon crystals contain enough magnetic minerals to be measured in the DC SQUID magnetometer. For the samples that had values of $M_{NRM} \geq 4 \times 10^{-12}$ Am^2 and $M_{IRM} \geq 4 \times 10^{-12}$ Am^2, the low-temperature magnetometry and microscopic observation revealed that the

zircon crystals contained magnetite and pyrrhotite. Combining the rock-magnetic parameter, we proposed the sample-selection criteria for future study of paleointensity experiments using single zircon crystals. In the case that the samples had high B_c values (>10 mT) or high M_{NRM}/M_{IRM} values (>~0.1), main remanence carriers are considered to be pyrrhotite, and these samples are inappropriate for the paleointensity study. In the case that the samples had low B_c values (<10 mT) and low M_{NRM}/M_{IRM} values (<~0.1), the main remanence carrier seems to be nearly pure magnetite with PSD grain sizes, and these samples are expected to be appropriate for the paleointensity study. The TRM acquisition experiments were also carried out on 12 of the zircon crystals that satisfied the above criteria (B_c < 10 mT and M_{NRM}/M_{IRM} < ~0.1). The ratios of NRM to TRM varied in the 0–2 range, thus indicating that the NRM intensity is comparable with that of TRM. The rough estimation of paleointensity using the bulk NRM/TRM ratio for the strong TRM sample showed a field intensity that was consistent with the geomagnetic field intensity at the Tanzawa tonalitic pluton for the last 5 Myr. Overall, the results from this study suggest that single zircon crystals of the Tanzawa tonalite would be applicable to paleointensity experiments.

Additional file

Sato *et al. Earth, Planets and Space* (2015) 67:150

Page 14 of 14

Author details
[1]Geological Survey of Japan, National Institute of Advanced Industrial Science and Technology, 1-1-1 Higashi, Tsukuba 305-8567, Japan. [2]Department of Environmental Changes, Faculty of Social and Cultural Studies, Kyushu University, 744 Motooka, Nishi-ku, Fukuoka 819-0395, Japan. [3]Department of Earth and Astronomy, Graduate School of Arts and Sciences, The University of Tokyo, 3-8-1 Komaba, Meguro-ku, Tokyo 153-8902, Japan. [4]Center for Advanced Marine Core Research, Kochi University, B200 Monobe, Kochi 783-8502, Japan. [5]Department of Earth and Planetary Sciences, Tokyo Institute of Technology, 2-12-1 Ookayama, Meguro-ku, Tokyo 152-8550, Japan. [6]Earth-Life Science Institute, Tokyo Institute of Technology, 2-12-1 Ookayama, Meguro-ku, Tokyo 152-8550, Japan.

References
Carter-Stiglitz B, Moskowitz B, Solheid P, Berquó TS, Jackson M, Kosterov A (2006) Low-temperature magnetic behavior of multidomain titanomagnetites: TM0, TM16, and TM35. J Geophys Res 111:B12S05
Day R, Fuller M, Schmidt V (1977) Hysteresis properties of titanomagnetites: grain-size and compositional dependence. Phys Earth Planet Inter 13:260–267
Dekkers MJ, Mattéi JL, Fillion G, Rochette P (1989) Grain-size dependence of the magnetic behavior of pyrrhotite during its low-temperature transition at 34 K. Geophys Res Lett 16:855–858
Dunlop SD (2002) Theory and application of the Day plot (M_{rs}/M_s vs. H_{cr}/H_c) 1. Theoretical curves and tests using titanomagnetite data. J Geophys Res 107(B3):EPM 4-1–EPM 4–22
Heider F, Dunlop DJ, Soffel HC (1992) Low-temperature and alternating field demagnetization of saturation remanence and thermoremanence in magnetite grains (0.037 μm to 5 mm). J Geophys Res 97(B6):9371–9381
Ishihara S, Kanaya H, Terashima S (1976) Genesis of the Neogene granitoids in the Fossa Magna region in Japan. Marine Sci Monthly 8:523–528
Ishihara S, Matsuhisa Y (1999) Oxygen isotopic constraints on the geneses of the Miocene Outer Zone granitoids in Japan. Lithos 46:523–534
Ishikawa Y, Saito N, Arai M, Watanabe Y, Takei H (1985) A New Oxide Spin Glass System of (1-x) FeTiO$_3$–xFe$_2$O$_3$. I. Magnetic Properties. J Phys Soc Jpn 54:312–325
Kawate S, Arima M (1998) Petrogenesis of the Tanzawa plutonic complex, central Japan: exposed felsic middle crust of the Izu–Bonin–Mariana arc. Island Arc 7:342–358
Kawate S, Fujimaki H (1996) Strontium isotope composition of the Tanzawa plutonic rocks in the Izu–Bonin arc. Japan Earth and Planetary Science Joint Meeting, Abstracts, Osaka, Japan, 703.
Kosterov A (2003) Low-temperature magnetization and AC susceptibility of magnetite: effect of thermomagnetic history. Geophys J Int 154:58–71
Lewis RR, Senftle FE (1966) The source of ferromagnetism in zircon. Am Mineral 51:1467–1475
Matsuda T (1978) Collision of Izu–Bonin arc with central Honshu. Cenozoic tectonics of the Fossa Magna, Japan. J Phys Earth 26:S409–S421
Moskowitz BM, Frankel RB, Bazylinski DA (1993) Rock magnetic criteria for the detection of biogenic magnetite. Earth Planet Sci Lett 120(3):283–300
Moskowitz BM, Jackson M, Kissel C (1998) Low-temperature magnetic behavior of titanomagnetites. Earth Planet Sci Lett 157:141–149
Muxworthy AR, Evans ME (2012) Micromagnetics and magnetomineralogy of ultrafine magnetite inclusions in the Modipe Gabbro. Geochem Geophys Geosyst 14:921–928

Niitsuma S, Niitsuma N, Saito K (2003) Evolution of the Komiji Syncline in the North Fossa Magna, central Japan: Paleomagnetic and K–Ar age insights. Island Arc 12:310–323
Özdemir Ö, Dunlop DJ, Moskowitz BM (1993) The effect of oxidation on the Verwey transition in magnetite. Geophys Res Lett 20:1671–1674
Rudnick RL, Fountain DM (1995) Nature and composition of the continental crust: a lower crustal perspective. Rev Geophys 33:267–309
Suyehiro K, Takahashi N, Ariie Y, Yokoi Y, Hino R, Shinohara M, Kanazawa T, Hirata N, Tokuyama H, Taira A (1996) Continental crust, crustal underplating, and low-q upper mantle beneath an oceanic island arc. Science 272:390–392
Suzuki K, Yamamoto S, Sawaki Y, Aoki K, Omori S, Kon Y, Hirata T, Li Y, Takaya Y, Fujinaga K, Kato Y, Maruyama S (2014) Zircon U–Pb dating from the mafic enclaves in the Tanzawa Tonalitic Pluton, Japan: Implications for arc history and formation age of the lower-crust. Lithos 196–197:301–320
Takahashi N, Kodaira S, Klemperer SL, Tatsumi Y, Kaneda Y, Suyehiro K (2007) Crustal structure and evolution of the Mariana intra-oceanic island arc. Geology 35:203–206
Takita R (1974) Petrography and plutonic history of the Tanzawa tonalite complex. Journal of the Geological Society of Japan 80:505–23 (in Japanese with English abstract)
Tamura Y, Ishizuka O, Aoike K, Kawate S, Kawabata H, Chang Q, Saito S, Tatsumi Y, Arima M, Takahashi M, Kanamaru T, Kodaira S, Fiske RS (2010) Missing oligocene crust of the Izu–Bonin arc: consumed or rejuvenated during collision? J Petrology 51:823–846
Tani K, Dunkley DJ, Kimura J, Wysoczanski RJ, Yamada K, Tatsumi Y (2010) Syncollisional rapid granitic magma formation in an arc-arc collision zone: evidence from the Tanzawa plutonic complex, Japan. Geology 38:215–218
Tarduno JA, Blackman EG, Mamajek EE (2014) Detecting the oldest geodynamo and attendant shielding from the solar wind: Implications for habitability. Phys Earth Planet Int 223:68–87
Tarduno JA, Cottrell RD, Davis WJ, Nimmo F, Bono RK (2015) A Hadean to Paleoarchean geodynamo recorded by single zircon crystals. Science 349:521–524
Tarduno JA, Cottrell RD, Nimmo F, Hopkins J, Voronov J, Erickson A, Blackman E, Scott ERD, McKinley R (2012) Evidence for a dynamo in the main group pallasite parent body. Science 338:939–942
Tarduno JA, Cottrell RD, Smirnov AV (2006) The paleomagnetism of single silicate crystals: recording geomagnetic field strength during mixed polarity intervals, superchrons, and inner core growth. Rev Geophys 44:RG1002
Tarduno JA, Cottrell RD, Watkeys MK, Hofmann A, Doubrovine PV, Mamajek EE, Liu D, Sibeck DG, Neukirch LP, Usui Y (2010) Geodynamo, solar wind, and magnetopause 3.4 to 3.45 billion years ago. Sience 327:1238–1240
Tauxe L, Bertram HN, Seberino C (2002) Physical interpretation of hysteresis loops: micromagnetic modeling of fine particle magnetite. Geochem Geophys Geosyst 3(10):1055
Yamada K, Tagami T (2008) Postcollisional exhumation history of the Tanzawa Tonalite Complex, inferred from (U-Th)/He thermochronology and fission track analysis. J Geophys Res 113:B03402
Yamamoto S, Nakajima J, Hasegawa A, Maruyama S (2009) Izu-Bonin arc subduction under the Honshu island, Japan: evidence from geological and seismological aspect. Gondwana Res 16:572–580
Yamamoto Y, Tsunakawa H (2005) Geomagnetic field intensity during the last 5 Myr: LTD-DHT Shaw palaeointensities from volcanic rocks of the Society Islands, French Polynesia. Geophys J Int 162:79–114
Yu Y (2010) Paleointensity determination using anhysteretic remanence and saturation isothermal remanence. Geochem Geophys Geosyst 11:Q02Z12
Yu Y (2011) Importance of cooling rate dependence of thermoremanence in paleointensity determination. J Geophys Res 116, B09101